3-3-5 Regional Reference Total Electron Content Model over Japan Using Solar EUV Proxies

MARUYAMA Takashi

Solar proxies and indices describing extreme ultraviolet (EUV) irradiance that affects the ionospheric total electron content (TEC) were examined through training an artificial neural network (ANN). A TEC database was constructed from a dense GPS receiver network over Japan from April 1997 to March 2008, covering an entire 11-year solar activity cycle. In the present study, ANN training for predicting TEC as a target parameter was done by including new solar proxies/indices in the input space that were based on direct measurements of solar EUV/UV flux, SOHO_SEM$_{26-34}$ (the integrated 26–34 nm EUV emission), and Mg II cwr (the core-to-wing ratio of Mg II 280 nm line), as well as the traditional indices $F_{10.7}$ and sunspot number. General improvements were obtained by combining different types of proxies and their short- and long-term means. The best combination was the 3-day smoothed daily, 7-day and 27-day backward mean values of Mg II cwr, SOHO_SEM$_{26-34}$, and the 10.7-cm radio flux.

Keywords
Total electron content, $F_{10.7}$, Sunspot number, Mg II cwr, SOHO_SEM$_{26-34}$

1 Introduction

The ionospheric total electron content (TEC) is a basic parameter that describes the status of the ionosphere. From the perspective of space weather forecasts, TEC is important in evaluating errors in the advanced use of GPS satellites stemming from delays in radio waves that propagate through the ionosphere. The major factor regarding changes in TEC is the change in flux of extreme ultraviolet (EUV) radiation 102.5 nm or less in wavelength that ionizes the neutral atmosphere. EUV flux that penetrates into the earth's upper atmosphere changes over various time scales. Among those time scales are the 11-year cycle of solar activity changes and the 27-day cycle of the sun's rotation, along with seasonal and daily variations due to the change in the solar zenith angle. Other important factors regarding changes in TEC include changes in the loss rate of ionospheric plasma due to changes in the neutral atmospheric (thermospheric) composition. The important loss process of O^+ (the major ion in the ionosphere) involves the dissociative recombination of molecular ions (NO^+ and O_2^+) produced in charge exchange due to the collisions with N_2 and O_2 (rearrangement collision). The dissociative recombination of these molecular ions progresses faster than the charge exchange process due to rearrangement collisions, so that the atmospheric composition ratio [O]/[N_2] greatly affects changes in TEC. The temperature and other conditions of the thermosphere significantly affect the atmospheric composition, and again, the thermosphere is governed by solar UV/EUV. At an altitude of 170 to 300 km, the ionization process of the neutral atmosphere due to EUV is the primary heat source[1]. Absorbed EUV energy is distributed into the photo electron energy and the chemical energy of ion-electron pairs, but the percentages thereof depend on the EUV wavelength. Eventually, photons with wavelengths shorter than 102.5 nm are all absorbed by the

atmosphere due to ionization[2]. The ionization cross sections of O, N_2, and O_2 have a broad peak near wavelengths of 40 to 70 nm. At shorter wavelengths, the ionization cross section becomes smaller and the energy absorption occurs at lower altitudes. At lower altitudes, the higher loss rate of ions makes the EUV contribution to the electron density relatively small.

In the region lower than an altitude of about 170 km, the primary heat source is the dissociation of O_2 by the far ultraviolet (FUV) radiation of the Schumann-Runge continuum (130 – 175 nm in wavelength). And since this process also affects the $[O]/[N_2]$ value, the FUV flux contributes to changes in electron density as well. In this way, solar ultraviolet radiation contributes to changes in TEC not only directly (through the ionization process) but also indirectly (through thermospheric changes). Since the relation between the solar ultraviolet radiation spectrum (covering a wide wavelength range) and TEC is extremely complex in this way, this paper does not consider particular wavelengths, but instead conceptually addresses the solar energy flux of ionospheric-effective EUV (IE-EUV) that contributes to the ionosphere. The purpose of this paper is therefore to examine IE-EUV behavior relative to various solar proxies, as pertaining to building an empirical TEC model.

Most solar ultraviolet radiation concerned here is absorbed by the earth's upper atmosphere, and data from satellite observations of solar ultraviolet radiation outside the atmosphere is not always obtainable. Therefore, many theoretical or empirical models of the ionosphere and thermosphere have been built to date using proxies. The representative ones are the sunspot number (R) and radio noise with a wavelength of 10.7 cm ($F_{10.7}$ index). One thermospheric empirical model — Mass Spectrometer and Incoherent Scatter Radar (MSIS)[3][4] — utilizes two parameters as proxies for heating due to ultraviolet radiation: the $F_{10.7}$ index on a given day and the average of 81 day period (i.e., three solar rotations) centered that day. On the other hand, the International Reference Ionosphere (IRI)[5] uses the 12-month average of sunspot numbers as a solar proxy. The EUV model for aeronomical calculations (EUVAC) developed by Richards et al.[2] provides the spectral intensity of ultraviolet flux by using a parameter as defined by the arithmetic average of the $F_{10.7}$ index on the day concerned and the 81-day mean of it.

In recent years, solar flux measurements as obtained by satellite instruments have been vigorously examined in connection with the upper atmosphere. It has become possible to use EUV flux data 26 – 34 nm in wavelength as obtained from the Solar Extreme Ultraviolet Monitor (SEM) onboard the Solar and Heliospheric Observatory (SOHO) satellite launched at the end of 1995 into orbit at the L1 Lagrange point. Regarding data obtained from SOHO_SEM, unlike other proxies, the observed wavelength range overlaps the wavelength range responsible to ionization of the earth's upper atmosphere as mentioned earlier. Bowman et al.[6] normalized the integrated flux of 26 – 34 nm from SOHO_SEM into a long-term change width of $F_{10.7}$ and introduced a new index ($S_{10.7}$) in order to make the flux input for an empirical thermospheric model. Another important solar proxy often applied is the core-to-wing ratio of Mg II (Mg II cwr). This uses the ratio of the absorption line center and both of its wings of Mg II close to a wavelength of 280 nm, as a proxy first proposed by Heath and Schlesinger to represent solar activity in the chromosphere[7]. Many researchers have examined the relation between Mg II cwr and changes in terms of ultraviolet radiation in other wavelength ranges and $F_{10.7}$ [8]–[12]. Emmert et al.[13] showed a good correlation between the Mg II cwr and integrated EUV energy in wavelengths of 0 – 120 nm from SEE observations on the TIMED satellite. Lean et al.[14] pointed out that this chromospheric activity index represents EUV flux more precisely than before by using it alone or combination with the $F_{10.7}$ index. In this way, many studies have shown that Mg II cwr is a good solar

proxy.

As shown by Floyd et al.[12], however, the Mg II cwr, $F_{10.7}$, R, and He 1083 solar indices exhibit different long-term variability. It is known that short-term variability over several rotational periods in these proxies differs as well[12][15]. These differences in behavior are partly due to the fact that the radiation of energy related to the respective observations is from different regions of the sun. In building up atmospheric models, Tobiska et al.[16] pointed out the importance of combined use of solar indices showing different behavior in connection with time changes.

Another important point to note in using solar proxies in an empirical model is the amplitude relation between long- and short-term changes. That is, the amplitude ratio of the 27-day periodic changes due to the sun's rotation and the 11-year solar cycle changes varies with the wavelength[17]–[19]. As a result, simply combining the short-term change component and long-term change component of a certain proxy cannot become an accurate proxy of IE-EUV. One attempt to address this issue was the method mentioned previously that combines the value of a given day and the average value over 81-day period centered on that day when using the $F_{10.7}$ index as a proxy of solar EUV[3][4].

The response to the solar flux variations is widely studied for the thermosphere as compared with the ionosphere. Changes in the thermosphere and those in the ionosphere due to changes in solar activity are strongly correlated, but the flow of energy is complex and not exactly the same[1], so that both changes could differ as well. For that reason, the solar proxies used to describe the ionospheric variation should not completely match those of the thermospheric variation. When we wish to examine the effects of solar activity on the ionosphere through a statistical approach, the advantage of SOHO_SEM$_{26-34}$ and Mg II cwr over other solar flux measurements is in the continuity of data. That is, data are obtained almost continuously over the 11-year solar cycle or more, and completely cover the period of our TEC data set. In this paper, the solar proxies pertaining to describe IE-EUV are examined from SOHO_SEM$_{26-34}$, Mg II cwr along with the conventional sunspot number and 10.7 cm radio intensity and combinations of those parameters. The output of the SOLAR2000 empirical solar irradiance model[20] is also evaluated.

Because the response of the ionosphere/thermosphere system to the solar inputs described by multiple proxies is extremely complex, we applied the artificial neural network (ANN) technique to examine input-output relationship. The most widely used ANN is a multilayer perceptron[21], and when it is applied to an ionospheric problem, directly observed quantity (such as foF_2, $h'F_2$, and TEC) becomes a target parameter. Input parameters include solar indices, the season, time of day (local time), latitude/longitude, and other factors that may affect the ionosphere. Since our initial goal was to find the optimal solar proxies, however, only the season and solar indices are in the input space, and other factors are embedded in the target parameter. Section **2** describes this ANN technique, section **3** compares the ANN learning results with regard to various proxies and the combination of them, and section **4** discusses the physical interpretations of the results. Section **5** compares the ANN predicted TECs with the observed TECs. Section **6** then gives a summary and discusses future prospects.

2 TEC Database and ANN Technique

In Japan, a dual-frequency GPS receiver network (GPS Earth Observation Network or GEONET) that covers the entire region of Japan was set up by the Geospatial Information Authority of Japan and has provided data ever since April 1997. For this period that spans one cycle of solar activity maximum and minimum, about 300 receivers being distributed uniformly from all GEONET receivers are chosen to evaluate TEC. The greatest challenge to address when evaluating

TEC from GPS signals received is a method of estimating the inter-frequency biases intrinsic to the satellite and receiver instruments and a method to convert the TEC along the oblique propagation path (slant TEC or sTEC) to vertical TEC (vTEC). Here, sTEC is converted into vTEC at the point where the propagation path crosses an altitude of 400 km (ionospheric piecing point), and the vTEC is assumed to be constant in a small cell of 2×2° latitude/longitude. Assuming that the inter-frequency biases remain constant during a 24-hr period, the TEC values were determined at 15-min intervals from a dataset of 24 hr. This technique is described in detail by Ma and Maruyama[22]. The values of each grid point or center of each cell determined in this way are referred to as grid TEC (gTEC). Figure 1 shows the distribution of the grid points used.

The major factors of TEC variations include solar activity, the season, time of day, and geographical/geomagnetic location. To deal with these multiple factors we applied an artificial neural network (ANN)[21][23]. The ANN approximates the relations between inputs (geophysical parameters in this case) and targets (observations such as TEC), and has often been used to predict the ionospheric parameters under given geophysical conditions[24]–[26]. In this study, however, the times of day and geographical/geomagnetic coordinates were embedded into the targets. Because we are interested in TEC variations in a limited longitude range over Japan, it is assumed that the time of day and longitude are exchangeable for each other, and that the displacement is constant between geomagnetic latitude and geographical latitude. Then we express the TEC variation with a two-dimensional distribution map of times of day and latitudes, which will be the target of the ANN.

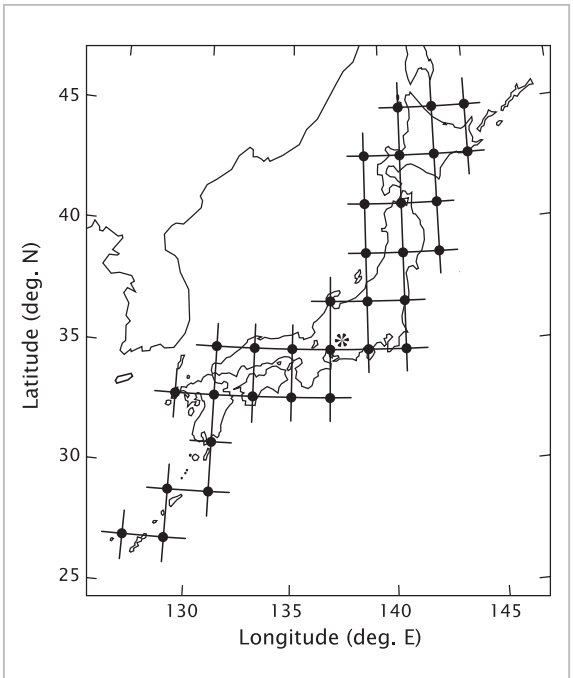

Fig. 1 *Grid points for which total electron content (TEC) was evaluated*

TEC is derived at 15-min intervals for each grid point. The values at the grid point marked * (35° N latitude, 137° E longitude) were used to evaluate learning of the neural network.

To generate a two-dimensional map of TEC, spherical functional expansion is used as follows:

$$\mathrm{TEC}=\sum_{m=0}^{M}\sum_{n=m}^{N}(A_{nm}\cos m\phi+B_{nm}\sin m\phi)P_n^m(\cos\theta) \quad (1)$$

Here, P is the associated Legendre function. The longitudinal parameter is the local mean time (LMT) corresponding to the longitude of each grid point, that is, $\phi=2\pi$ (LMT/24), θ is colatitude, and $N = M = 7$. In the equation, determining A_{nm} and B_{nm} with the least square fitting provides a TEC map. The coefficients here will therefore be adopted as actual target parameters. For mathematical convenience, the regions outside 29 to 45° are extrapolated and the southern hemisphere with no data is provided with dummy data to ensure north-south symmetry to obtain functional approximation, so that the coefficients with an odd number of $n + m$ become zero. Therefore, a total of 36 targets (i.e., nodes of the output layer) are required to express a two-dimensional TEC map. The two-dimensional daily map is prepared based on three days' worth of TEC data and takes a moving average. Data were processed for 11 year from April 1, 1997 to March 31, 2008, which will become a dataset for ANN learning and evaluation.

For the four representative seasons of

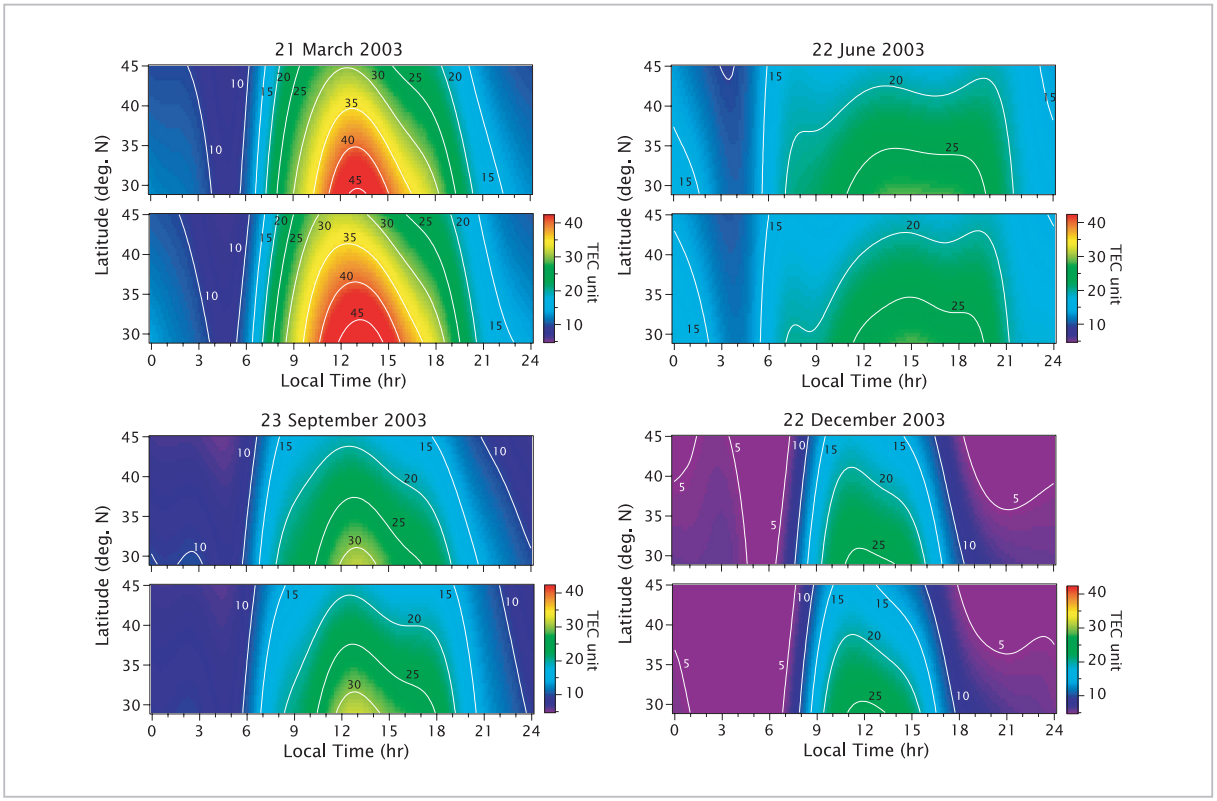

Fig.2 *Map of time-latitude variations in TEC represented by spherical function expansion for typical seasons*

The top row for each season indicates the outputs of the neural network; the bottom row indicates the observed values.

2003, Fig. 2 shows an example of a TEC map. For each season, the bottom row indicates observed values and the top row indicates the outputs from the trained ANN as stated below.

Figure 3 shows the configuration of the ANN: 36 nodes for the output layer and 100 nodes for the hidden layer, with the number of nodes in the input layer being changed from 3 to 18 according to the combination of solar proxies. Learning of the ANN is conducted as divided in two stages. First, pattern mode[21] is used where the weight of neurons is updated every time one set of inputs and target data are given. After some convergence, batch mode[21] is then used for learning where the weight is updated after all 11 years' worth of data is given. In the batch mode, the learning constant and moment were set to 0.9. Teacher data and ANN outputs for the 36 nodes were compared and their square errors are evaluated over the period of 11 years. The learning was completed when the change in square error for each weight update becomes 10^{-5}. Since batch mode learning generally involves the smooth behavior of error convergence, it would be suited for comparative evaluation of the input parameters like in this study. The batch mode

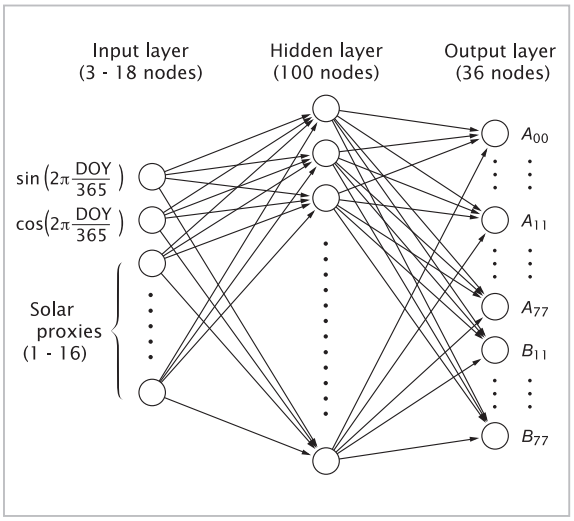

Fig.3 *Configuration of the neural network*

leaning applied to a quite large amount of dataset in this study was realized by using the target parameters converted into a two-dimensional map.

To evaluate the achievement of the learning, the whole dataset over 11 years was divided into two subsets for learning and evaluation. At that time, to enable the learning and evaluation subsets to cover all the phases of solar activity and the seasonal changes of the ionosphere without missing anything, data for evaluation was extracted at a rate of once every ten days and the rest was used for learning. Learning results were not evaluated directly with respect to the target parameters (Legendre coefficients), but by reconstructing a TEC map from the coefficients and determining the root mean square error (RMSE) for the hourly values of TEC using the evaluation dataset. In learning of the ANN, the initial weight for each neuron is given as a random number. For that reason, the learning results vary not only according to how solar proxies are selected but also according to the initial weights given. Moreover, evaluation is conducted with a reconstructed TEC map, so that the best evaluation (i.e., minimum RMSE) of all 11 independent runs of leaning was regarded as the degree of achievement in conducting an even more accurate comparative evaluation.

The solar proxies to be compared are the sunspot number, 10.7 cm solar radio noise, 26–34 nm integrated EUV flux from SOHO_SEM, and Mg II cwr. The sunspot number used is the International Sunspot Number (R_i) statistically calculated by the Solar Influences Data Analysis Center (SIDC) of Belgium based on a global observation network. The 10.7 cm radio noise index ($F_{10.7}$) is the value observed at 20:00 UT in Penticton, Canada. This value has been continuously observed for a long time with high accuracy and is highly evaluated as a standard dataset. As the input and target parameters must be normalized to take values between 0 and 1 in the actual ANN calculation, the values of R_i and $F_{10.7}$ were divided by each maximum during the 11-year period. Mg II cwr is observed twice a day by the NOAA satellite. The SOHO_SEM observation equipment observes EUV intensities of 26 – 34 nm with an even higher time resolution; thus a 24-hour average is used. Tobiska et al.[16] preprocessed these observed values of ultraviolet radiation and produced the $M_{10.7}$ and $S_{10.7}$ daily indices scaled to have the same long-term variation with the $F_{10.7}$ index. In the ANN calculation, the $M_{10.7}$ and $S_{10.7}$ values were divided by the each maximum during the 11-year period. SOHO_SEM has periods where data were missing, and these portions were complemented after being compared the data before and after the deficient portion with the S_{euv} index obtained from the SOLAR2000 empirical solar irradiance model. The composed index is referred to as $S^*_{10.7}$.

The SOLAR2000 model (http://www.spacewx.com/solar2000.html) is an empirical model of solar ultraviolet spectral intensity based on Lyman α and $F_{10.7}$ as inputs[20]. The S_{euv} index is an integrated SOLAR2000 EUV intensity at the wavelengths of 26–34 nm, which corresponds to the SOHO_SEM measurements. In addition to the S_{euv} index, the integral value $E_{10.7}$ of 1–105 nm related to ionization of the earth's upper atmosphere is also calculated. These two indices are also evaluated as inputs to the TEC ANN model, similarly to the indices based on observations.

As previously described, a TEC map was prepared as the average of three days. A three-day average (called the daily value for the sake of convenience) will be used for solar indices too. In addition to the solar indices of a given day, the means of 7, 27, and 81 days going back to the past from the date of the TEC value (backward means) and the means of 7, 27, and 81 days centering on the date of the TEC value (center means) are examined on their functions as ANN inputs. Here, the 27 and 81 days correspond to one and three solar rotations, respectively, and the mean of the seven previous days (a quarter solar rotation) is intended to examine the integrating effects of thermospheric and ionospheric responses to

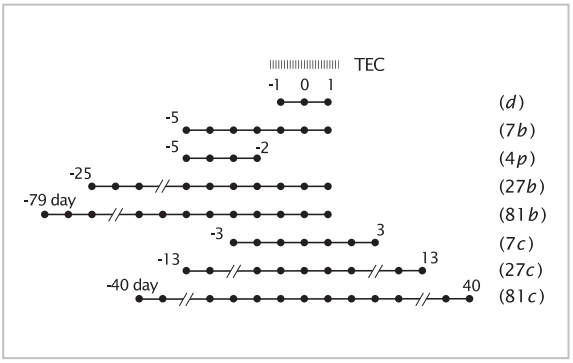

Fig.4 *Periods for averaging short-term changes*

IE-EUV variation. To verify the effects of integration, consideration is also given to the values produced by dividing the backward mean of seven days into three and four days. Figure 4 summarizes the period during which these mean values were obtained. Six solar indices and their respective means during eight periods yield 48 parameters. This means that, in principle, $2^{48}-1$ ($\sim 10^{14}$) combinations are possible. Moreover, in considering those time delays as well, the combination patterns of input parameters become even more numerous. Needless to say, trying all those combinations is not realistic. In this paper, ANN learning and the results for about 300 combination patterns were evaluated by progressively narrowing down from a single parameter to a maximum of 16 (4 indices × 4 period means).

3 Results

3.1 Comparison of single proxy

The use of a single solar index as a proxy for IE-EUV is the most elementary way of modeling TEC. Figure 5 compares the five indices. The zero on the horizontal-axis represents the index on the same day as the date TEC was observed. Then, the negative (positive) numbers mean that a solar index on a prior (later) date by the number indicated. RMSE on the vertical-axis is the achievement of the ANN learning; the smaller the number, the more suitable proxy for TEC modeling. As known by past studies, the sunspot number is the least suitable for describing IE-EUV variation. The $F_{10.7}$ index yielded a better result than the sunspot number, but RMSE is still high. The best result was in the case of SOHO_SEM$_{26-34}$, which is quite natural if we consider that the wavelength range observed overlaps the wavelength range of EUV that contributes to atmospheric ionization. Mg II cwr, which is observed at 280 nm wavelength outside the wavelength range that contributes to ionization, yielded a result between $F_{10.7}$ and SOHO_SEM$_{26-34}$. For comparison with SOHO_SEM$_{26-34}$, S_{euv} from the SOLAR2000 model is shown by the dotted line and generally exhibits good performance, although the curve is somewhat flat when compared with that of SOHO_SEM$_{26-34}$.

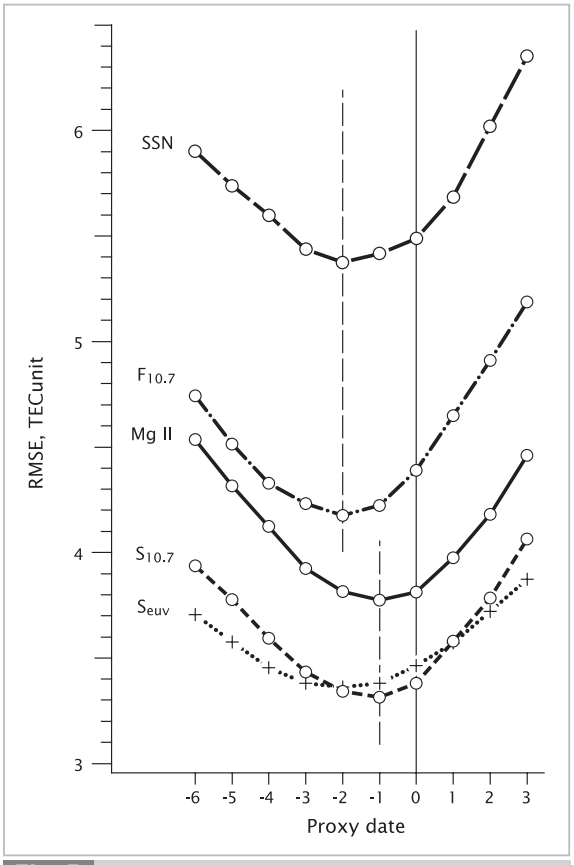

Fig.5 *Learning results for individual proxy when using a daily parameter alone*

A response delay of one to two days is seen.

It has been known that changes in the earth's upper atmosphere indicate a delayed response of several days to changes in solar EUV. As shown in Fig. 5, the optimal leaning

result also has a time delay. This delay in time varies among different proxies. With regard to R_i, $F_{10.7}$, and S_{euv} from the SOLAR2000 model, the learning achievement is highest when using the proxy value obtained 1.5 to 2 days prior to the date of TEC value. For $S_{10.7}$ and $M_{10.7}$ based on the observations of ultraviolet radiation, the learning achievement is highest when the time delay is one day.

3.2 Improvement by short-term means

Figure 6a shows the results of the combined use of several short-term means with the daily index a day prior to the date of TEC observation (in considering the delay in ionospheric response described above) as ANN inputs. The horizontal axis is a combination of short-term periods in which mean value is taken as indicated in Fig. 4. Here, 1 denotes the daily index (d) alone in the input space, 2 the result of including the 7-day backward mean (d + 7b) in the input space, 3 the result of including the 27-day backward mean further (d + 7b + 27b), and 4 the result of including all the 7-, 27-, and 81-day backward means (d + 7b + 27b + 81b). Although increasing the number of input parameters generally improves learning, the effects thereof show some differences according to the proxy used. The sunspot number and $F_{10.7}$ show a clear improvement with increasing in the number of parameters, and the best result was obtained with combination 4. On the other hand, Mg II cwr shows that combination 3 is best, and adding the 81-day mean yields, rather, a worse result. The $E_{10.7}$ and $S^*_{10.7}$ indices do not show any significant improvement, even when using short-term mean values in combination, which may implies that the index of the current day alone fairly well describes changes in EUV compared with the other proxies.

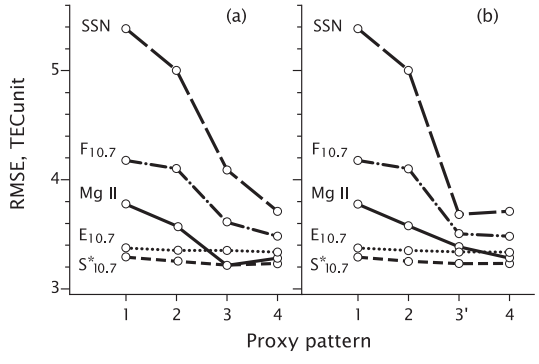

Fig.6 *Improvement of learning when combining the averages from different periods for each proxy*

Figure 6b is the same as Fig. 6a except that combination 3 is replaced by 3´. In combination 3´, the 7-day backward average and 81-day backward average are used (d + 7b + 81b). The figure reveals that, for the sunspot number, the 81-day average has a great effect and adding the 27-day average produces rather a worse learning result. For $F_{10.7}$, the 81-day average is also highly effective and adding the 27-day average hardly shows any advantage. Summarizing Figs. 6a and 6b, we found that longer-term average behavior is important for the sunspot number and $F_{10.7}$ as IE-EUV proxies, and that it is a little shorter and the 27-day average is important for the UV observation-based indices, $S^*_{10.7}$ and Mg II cwr.

So far we have examined backward averages with period of several days. However, previously constructed empirical models have used period averages centering on the day of measurements of TEC or other ionospheric parameters. Thus we further examined cases when centered averages were used instead of backward averages and the results are compared in Table 1. The numbers and symbols describe the combinations are those shown in Fig. 4. In both the cases backward and centered averages were used, the 81-day averages are generally important for the sunspot number and $F_{10.7}$, and the 27-day averages for $M_{10.7}$. For each proxy, no major difference was noted between the backward average and center average except that the backward average is better for the sunspot number. It should be noted that these results are the case when proxy averages are used as an ANN inputs in combination with the daily value. If the averages alone are examined, the centered averages should show larger correlation with the measurements.

Table 1 Comparison between backward average and central average

proxy	Combination pattern[(1)]				
	d	*d*+27*b*	*d*+27*c*	*d*+81*b*	*d*+81*c*
R_i	5.38	4.05	4.29	3.72	3.94
$F_{10.7}$	4.18	3.54	3.67	3.48	3.48
$M_{10.7}$	3.77	3.26	3.26	3.41	3.30
$S^*_{10.7}$	3.28	3.23	3.24	3.23	3.27

(1) For the meaning of each variable, see Fig. 4.

3.3 Combination of different proxies

In the above examinations, the input solar parameters, daily and averages over several periods, were a single kind of index. In the next step, we examined how the learning efficiency is improved when different proxies are jointly used. Table 2 lists the learning results for combinations of various proxies. The first four lines in the table (Run 1-1 to 1-4) reproduce the results of single proxies for comparison. The subsequent six lines (Run 2-1 to 2-6) show results of a combination of two different proxies, the next two lines (Run 3-1 and 3-2) show a combination of three proxies, and the last one (Run 4-1) is the case all proxies are combined. Looking at the effects of combining the sunspot number and $F_{10.7}$ shows that Run 2-6 produced better results than when using these respective proxies alone (Run 1-1 and 1-2). However, combining the sunspot number and $S^*_{10\text{-}7}$ or $M_{10.7}$ produces slightly worse results than when using these indices based on UV measurements alone, and it is shown here again that the sunspot number is inferior as a solar proxy. The combination of other proxies aside from the sunspot number always produced good results, and combining $S^*_{10.7}$ proved particularly effective. Next, combining three or four proxies again produces good results when excluding the sunspot number. The use of nine total parameters of *d*, 7*b*, and 27*b* for $F_{10.7}$, $S^*_{10.7}$, and $M_{10.7}$ (Run 3-2) was the best input pattern in all cases.

Table 2 Combination effects of different proxies

Run	proxy				RMSE
	R_i	$F_{10.7}$	$S^*_{10.7}$	$M_{10.7}$	
1-1	✓				4.09
1-2		✓			3.61
1-3			✓		3.22
1-4				✓	3.21
2-1	✓			✓	3.23
2-2		✓		✓	3.20
2-3			✓	✓	3.16
2-4	✓		✓		3.24
2-5		✓	✓		3.17
2-6	✓	✓			3.52
3-1	✓		✓	✓	3.16
3-2		✓	✓	✓	3.12
4-1		✓	✓	✓	3.16

Each proxy consists of *d*, 7*b*, and 27*b* from Fig. 4.

4 Interpretation of Results

4.1 Time delay in ionospheric response

The solar proxies best suited for modeling TEC variations brought about by changes in solar EUV input (IE-EUV) were evaluated by using the ANN technique. As a precondition, when the input parameter for the ANN correlates closely with the target parameter, then the error (RMSE) between the trained ANN outputs and observed values is assumed to decline. Wu and Lundstedt[27] examined the relation between changes in the solar wind

parameter and geomagnetic storms with a similar ANN technique, and showed that a comparison of RMSE of the ANN would not contradict a comparison of the correlation coefficient. The delay in TEC response to solar activity changes shown in Fig. 5 can also be compared with the results of correlation analysis. Jacchia et al.[28] and Paul et al.[29] examined changes in satellite orbit and found that there is a delay of one to two days in changes in thermospheric density relative to the modulation of solar ultraviolet intensity with the 27-day period. The series of MSIS empirical thermospheric models[3] also use the $F_{10.7}$ index of the preceding day. Bowman et al.[6] use the values one day before for $F_{10.7}$ and $S_{10.7}$, and the value five days before for $M_{10.7}$ in their thermospheric density model. Similarly, a delay in ionospheric response to solar activity changes has also been reported[30]–[32]. Min et al.[32] conducted a correlation analysis of how thermospheric density and TEC respond to solar activity changes, and their Fig. 6 showing correlation strengths looks very similar to Fig. 5 in this paper when rotated 180 degrees. Thus, the characteristics of time delay shown in Fig. 5 basically match those of previous analyses and endorse the appropriateness of comparative analysis based on ANN-RMSE.

A detailed look at the time delay in TEC response to solar activity changes shows quantitative differences from past studies and differences among the proxies used in the present study. For any quantitative discussion on the time delay, we must pay attention to the representative time or time tag, T, of each proxy. A radio noise intensity of 10.7 cm wavelength was observed at 20:00 UT. While the daily value of $S_{10.7}$ is determined by averaging the values observed by the SOHO_SEM instrument at five-minute intervals. Similarly, observations made at 07:00 and 16:00 UT were used to determine the daily value of Mg II cwr. R_i is calculated by statistically processing the results of the global observation network, but the time represented is not explicitly indicated. On the other hand, the TEC data we used is obtained from an area centering on 135° E longitude, therefore the solar activity at around 03:00 UT (12:00 LT) might mostly contribute to the ionization.

Considering the time that represents each proxy, the time series of daily $F_{10.7}$ (T = 20:00 UT) is predicted to show a delay of eight more hours than that of $S_{10.7}$ and $M_{10.7}$ (T = 12:00 UT). However, Fig. 5 shows that the apparent response delay in TEC with regard to $F_{10.7}$ is about one day longer than that of $S_{10.7}$ and $M_{10.7}$. And although R_i is slightly shorter than $F_{10.7}$, it shows a longer response delay than $M_{10.7}$ and $S_{10.7}$. Regarding such response delay, two possibilities are considered. The first one is the integration effect on the thermospheric and ionospheric modification; the other is the characteristics of the solar proxies themselves. The wavelength of EUV that creates $S_{10.7}$ overlaps the wavelength range where the neutral atmosphere is ionized, so that the response delay regarding $S_{10.7}$ and $M_{10.7}$ is considered due to the characteristics of the thermospheric/ionospheric system. The excess delay time in $F_{10.7}$ and R_i is considered caused by solar activity observed with 10.7-cm radio waves or white light that growths and decays with a different time scale from IE-EUV activity. Donnelly et al.[33] and Floyd et al.[12] cite several episodes in which the short-term variation in sunspot number and 10.7-cm radio intensity actually reaches their peaks earlier than UV/EUV. Correlation analysis of $F_{10.7}$ and the sunspot number with UV flux of 205 nm (all which show 27-day modulation of the sun's rotation) revealed that $F_{10.7}$ and the sunspot number have a strong correlation with UV flux values of the previous rotation period[15]. This asymmetry relative to zero time lag in correlation between the UV flux and $F_{10.7}$ is because the lifetime of plages on the solar surface is longer than the lifetime of the sunspot number.

The SOLAR2000 empirical solar irradiance model uses the $F_{10.7}$ index as a proxy of corona activity and the intensity of Lyman α flux as a proxy of chromospheric activity. In Fig. 5, the response delay time of S_{euv} (i.e.,

SOLAR2000 output corresponding to $S_{10.7}$) is closer to that of $F_{10.7}$ rather than $S_{10.7}$. It is presumably due to the characteristics of $F_{10.7}$.

4.2 Improvement by combining short- and long-term components

Hedin[34] found that the inclination of a linear regression line between $F_{10.7}$ and EUV differs between short- and long-term changes. Donnelly et al.[17] also pointed out that the relation between the amplitude of long-term changes and that of short-term ones varies according to wavelength used to measure the solar activity. From these findings, extending short-term change characteristics to long-term changes to estimate IE-EUV by using proxies will be a major cause of error[19][35]. One method of compensating for differences in the short-term and long-term change amplitude characteristics of proxies used in MSIS and other atmospheric models is to use two parameters; an average over three solar rotation periods in addition to the index of the date to be determined. As the result of comparing the center averages (during the period centering on the target date) of 54, 81, and 108 days for $F_{10.7}$, $M_{10.7}$ and $S_{10.7}$ when developing their thermospheric temperature model, Bowman et al.[6] concluded that a center average of 81 days best expressed the long-term change component.

The ANN model discussed in this article also yielded improvement as shown in Fig. 6 by adding short-term change and long-term change components in the input space. However, the pertaining period for the long-term change components that yield improvements varies according to the proxies used as shown in Table 1: While the 81-day average was most effective for R_i and $F_{10.7}$, the 27-day average was effective for $M_{10.7}$ and $S_{10.7}$ based on UV measurements. Although the center average was considered appropriate in previous models, no significant difference was found between the backward average and center average. When running a model on a real-time basis, a model that uses the backward average based solely on observations is clearly advantageous over models using the center average, which entails the use of predictions as well.

Changes in solar ultraviolet radiation are characterized by the active network dispersed in the longitudinal direction and the localized plages. Short-term changes consist mainly of solar rotational modulations in energy flux stemming from localized plages. To even longer-term changes, both plages and the network contribute[36]. Woods et al.[19] stated that the active network's contribution to irradiance changes is larger from the transition region than from the chromosphere. Therefore, the ratio of long-term change components and short-term change components varies according to the activity of the solar atmospheric region represented by the proxies. With the progress of active regions, it takes one to three solar rotation periods for plages to decay into the active network and disperse in the longitudinal direction. The active network then remains present over several other solar rotation periods[19]. Donnelly et al.[15] and Lean and Repoff[37] analyzed the developments in sunspot number, $F_{10.7}$, and UV intensity over time, and found that the sunspots and $F_{10.7}$ have larger components of periods longer than the 27-day variation when compared with UV intensity. The results shown in this paper indicate that when compensation is made for differences between the short-term change and long-term change components among the proxies and IE-EUV, the 27-day average is sufficient for UV/EUV from the persisting active network, while data over 81 days must be averaged for the sunspot number and $F_{10.7}$, which show greater changes. Figure 6 shows that adding long-term change components to $E_{10.7}$ and $S_{10.7}$ will not considerably improve ANN learning, so that for these proxies, the relation between the short-term and long-term change components would be similar to that of IE-EUV.

4.3 Improvement by combining different proxies

IE-EUV responsible to ionization of the earth's upper atmosphere is emitted from the

chromosphere, transition region, and corona, and the contributions of each region to short- and long-term changes are different to each other. This is because the contrast between the active network and plages varies according to the region of the solar atmosphere[19]. Therefore, combining several proxies that represent different sources of radiation in solar atmospheric layers is effective in more accurately expressing changes in IE-EUV.

Mg II cwr exhibits very similar changes in radiation from the chromosphere and is considered a good proxy of chromospheric activity (see Reference[19]). The major contribution to SOHO_SEM$_{26-34}$ is the He II emission line (30.4 nm) of the transition region and the Fe XV emission line (28.4 nm) of corona. Radio waves at wavelength of 10.7 cm are considered to stem mainly from the transition region and corona[18]. Detailed discussion of the regions represented by the proxies is beyond the scope of this paper, but it is important to combine several proxies exhibiting as different behavior as possible when describing activity in the solar atmosphere over a wide range. In that sense, it is understood that using $F_{10.7}$, $M_{10.7}$, $S_{10.7}$, and a combination of some of their period averages has produced the best ANN learning results.

4.4 Roles of the 7-day backward average

The delay in response of the earth's upper atmosphere to changes in solar irradiance is a well-known phenomenon[6][28]–[32][38][39], and it is reconfirmed in this article as depicted in Fig. 5. This response delay is considered to emerge due to a combination of changes in solar flux having a 27-day period modulated by solar rotation along with the accumulation effects on the earth's upper atmosphere. When the average (actually the 7-day backward average) of proxies over a period shorter than the solar rotation period and longer than three days was added to the input space, the ANN is expected to learn the accumulation effects. In Fig. 6, the second point from the left for each proxy may actually represent accumulation effects. To examine this more in detail, several short-period averages were applied to conduct ANN learning. Table 3 lists the results. Here, the codes used for the proxies are as shown in Fig. 4, and the combinations of proxies include $F_{10.7}$, $S^*_{10.7}$, and $M_{10.7}$ in all cases. As is evident from the table, when an average over a period shorter than the 27-day rotation period was not used in combination (Run 5-2), the degree of learning achievement declined. Even the 7-day center average (Run 5-3) was not enough. Since the average over 4–7 days before (Run 5-1) produced the same results as the 7-day backward average (Run 3-2), some accumulation effects are presumed to be learned.

Another effect considered to be the role of the 7-day backward average is the possibility of learning limb darkening/brightening effect (changes in brightness in the periphery of the sun). Donnelly et al.[17] discussed how flux from the activity region (toward the earth) changes according to its distance from the central meridian (central meridian distance or CMD). This CMD characteristic varies according to the wavelength, and optically

Table 3 *Role of short-term mean*

	Proxy pattern*					
Run	*d*	4*p*	7*b*	7*c*	27*b*	RMSE
3-2	✓		✓		✓	3.12
5-1	✓	✓			✓	3.12
5-2	✓				✓	3.19
5-3	✓			✓	✓	3.14
5-4	✓	✓		✓	✓	3.12

*Common to $F_{10.7}$, $S^*_{10.7}$ and $M_{10.7}$

thick radiation attenuates greatly in the periphery and has a narrow CMD characteristic[17][40][41]. When the proxies used are based on an optically thick emission line, IE-EUV is estimated at a lower level as the activity region comes closer to the periphery. As a result, when CMD information on the activity region is given, the ANN model is expected to improve. Table 3 presumably includes such effects, but the error caused by other factors (disturbances due to magnetic storms and the effects from lower atmosphere) as discussed in the next section limits the lower values of RMSE, and removing these causes of error is expected to clarify the faint effects such as the CMD characteristic.

5 Comparison of ANN Predictions with Observed Values

Figure 2 shows TEC maps for typical seasons. For each season the top row is a TEC map reconstructed from the coefficients of ANN outputs and the bottom row is a TEC map based on observations. Here, one can see that seasonal changes of local time and latitudinal characteristics are well reproduced by the trained ANN, and which proves that the combination of the spherical functional approximation and ANN is appropriate to model TEC variations.

Figure 7a compares the ANN outputs and observations on a day-to-day basis spanning 30 solar rotation periods: The ANN inputs included the nine solar parameters (i.e., 3-, 7-, and 27-day backward averages for $F_{10.7}$, $S^*_{10.7}$, and $M_{10.7}$) that produced the best learning results. The data compared here are the ANN output results for 35° N latitude and 03:00 UT (12:00 LT), and the corresponding observations at the grid point marked * in Fig. 1. The top panel in the figure shows the ANN (solid line), observed values (○), and the difference (ΔTEC); the middle panel shows the proxies used (only the 3-day running averages are shown); the bottom panel shows the A_p index

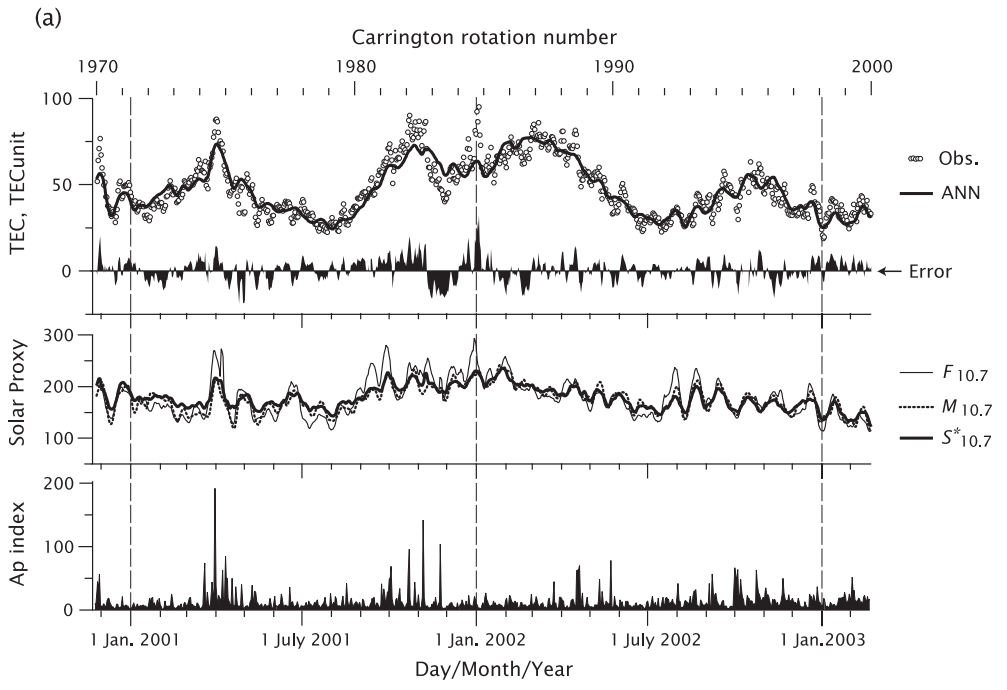

Fig.7a *Comparison of day-to-day variations in observed values and neural network outputs for the solar maximum period*

The top panel shows the total electron content obtained in observations (open circles) and in the neural network (solid line), and their differences (line filled to zero). The middle panel shows the solar proxies used for the neural network training (only the 3-day boxcar averages indicated), and the bottom panel shows the geomagnetic activity index.

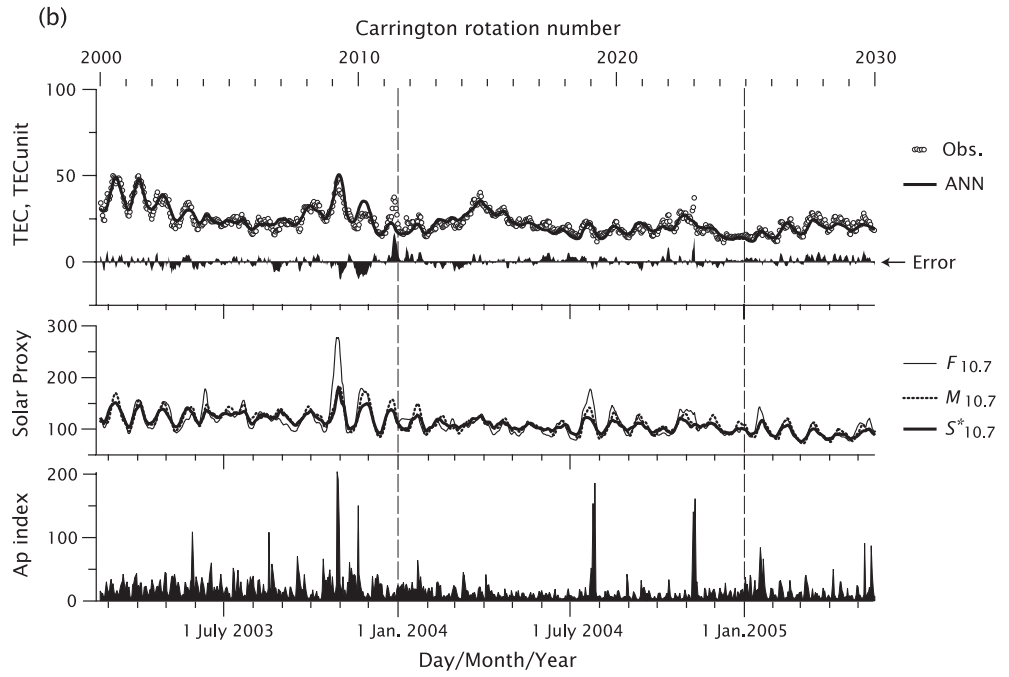

Fig.7b *The same as Fig. 7a but for solar medium period*

representing geomagnetic disturbances. One can see that a gradual seasonal trend and 27-day solar rotational changes in TEC are well reproduced by the model. However, errors may sometimes arise. Some of these errors are associated with a geomagnetic disturbance as characterized by the increase in the A_p index, but some others have no clear connection with geomagnetic disturbances. The largest geomagnetic disturbance in this period occurred on March 31, 2001 and several moderate geomagnetic disturbances occurred continually during a month around that date. A weak positive ionospheric storm was reported to have occurred associated with the largest geomagnetic storm and several strong negative ionospheric storms associated with other magnetic disturbances in this period[42]. These ionospheric storms can be found as ANN prediction errors in the plot of ΔTEC. The second largest geomagnetic disturbance occurred on November 6, 2001, at which time an extreme enhancement was seen in TEC (called the "TEC storm")[43]. However, for the period from November 7 to 24, it is difficult to connect the persisting negative ΔTEC to geomagnetic disturbances. Therefore, any changes in TEC corresponding to the geomagnetic disturbance on November 24 (the third largest disturbance of that period) are not clearly identified. The large positive and negative ΔTECs observed from January to February 2002 do not correspond to geomagnetic disturbances.

Figure 7b shows the data for the next 30 solar rotation periods, during which the solar activity has declined to a medium level. Negative ΔTEC is seen in response to the major geomagnetic disturbance during October 29 to 31, 2003 (called the "Halloween storm"). One solar rotation period later, around November 20, the negative ΔTEC continued for at least ten more days, so that it is difficult to simply link this long-duration negative event to geomagnetic disturbances this time. The major ΔTEC at the end of December 2003 cannot be linked to geomagnetic disturbances either. Hardly any TEC prediction error was seen on July 27, 2004 which is the date of the second largest geomagnetic disturbance of that period. The spike-like positive ΔTEC on November 8, 2004 was due to a geomagnetic disturbance, and this was also a very special event

in which an extremely intense positive ΔTEC called storm enhanced density (SED) was first recognized in Japan after sunset[44].

As shown above, geomagnetic disturbances often increase the TEC prediction error of the ANN by resultant ionospheric storms. But errors due to other causes are not necessarily small. A further examination of Fig. 7 shows that there often find quasi-periodical changes in the error amplitude. Although it cannot be denied that the proxies used here do not sufficiently represent the IE-EUV variations, these periodic errors might be ascribed to the coupling with the lower atmosphere[45][46]. This also implies that analyzing the behavior of ΔTEC in which solar influences are removed could help elucidate the possible coupling of ionosphere to lower atmosphere. That is why we call this model the reference model. By clarifying the changes in TEC that is driven by the lower atmosphere, the results can be fed back to further improve the TEC prediction model. This clarification and incorporating the effects of geomagnetic disturbances into the prediction model pose the next challenge to be addressed.

6 Summary and future prospects

By using the method of the artificial neutral network (ANN), a reference model was developed for the ionospheric total electron content (TEC) that is controlled by solar activity and the season. As the result of the examination of several indices used as solar proxies, the best learning results were obtained when the 10.7-cm solar radio noise index ($F_{10.7}$), Mg II cwr ($M_{10.7}$), and the value of 26 – 34 nm integrated EUV flux by the SOHO satellite ($S_{10.7}$) were used. From the time series of each index three parameters were computed, i.e., averaged for 7- and 27-day periods preceding the day of TEC observations as well as daily index (actually this is a three-day average corresponding to the three-day averaged TEC values as a target parameter), and thus 9 parameters were used as a solar input in total. Further, when these solar parameters were shifted by one day backward, corresponding to the delayed response of the ionosphere to the solar inputs, the best result was obtained. Based on the results of many past studies on solar radiation, a discussion was held on the physical significance of the input parameters used. The model developed here is based on solar indices preceding the dates concerned, so that the model can be readily applied to real-time TEC predictions (space weather forecasts). In this version, only changes in solar activity and seasonal controls were modeled, so that the model can also be a reference for evaluating ionospheric storms due to geomagnetic disturbances and examining possible coupling with the lower atmosphere. In the next step, it is necessary to improve the model as a prediction tool for further space weather applications, by incorporating those effects of ionospheric storms and coupling with the lower atmosphere.

To allow the model to learn the ANN efficiently, the distribution of TEC over Japan was expressed in the form of a spherical functional expansion. This method of expression is advantageous not only because it affords high learning efficiency for the ANN but also can convey desired TEC predictions of latitude, longitude, and time of day by using 36 Legendre's coefficients alone. Another conceivable application is the broadcasting of prediction results as correction information about ionospheric delay errors from positioning/navigation satellites as superimposed on positioning signals.

Yet another future challenge to be addressed is the development of a new index. TEC prediction with the ANN has become possible, but the ANN is not necessarily a general method, and the fact that it needs multiple input parameters (9 parameters in this model) for solar proxies alone inhibits its widespread application. From Fig. 6, the $F_{10.7}$ index is found to also excel as a proxy for IE-EUV when combined with several periodic averages than when using daily Mg II cwr alone. Searching for a functional form, which is not explicit in the ANN, should be able to

produce a new corrected index from time series of the $F_{10.7}$ value. Regarding $F_{10.7}$, data has been obtained over a far longer period than the indices based on UV/EUV observations; therefore, deriving a new corrected index is expected to be applicable to a long-term trend analysis of the earth's upper atmosphere and other applications. The prototype of this corrected index is already completed and its elaboration and evaluation are future challenges to be addressed.

Acknowledgments

The Solar Influences Data Analysis Center, WDC for the Sunspot Index, Royal Observatory of Belgium provided the sunspot numbers. The 10.7-cm solar radio flux index was observed at the Dominion Radio Astrophysical Observatory, Canada, and provided by the National Geophysical Data Center, NOAA, USA. The proxies $M_{10.7}$, $S_{10.7}$, S_{euv}, and $E_{10.7}$ were obtained from the Solar Irradiance Platform (SIP), and downloaded from the SIP quick link at http://spacewx .com.

References

1 R. S. Stolarski, P. B. Hays, and R. G. Roble, "Atmospheric heating by solar EUV radiation," J. Geophys. Res., Vol. 80, pp. 2266–2276, 1975.

2 P. G. Richards, J. A. Fennelly, and D. G. Torr, "EUVAC: A solar EUV flux model for aeronomic calculations," J. Geophys. Res., Vol. 99, No. A5, pp. 8981–8992, 1994.

3 A. E. Hedin, J. E. Salah, J. V. Evans, C. A. Reber, G. P. Newton, N. W. Spencer, D. C. Kayser, D. Alcaydé, P. Bauer, L. Cogger, and J. P. McClure, "A global thermospheric model based on mass spectrometer and incoherent scatter data, MSIS 1. N_2 density and temperature," J. Geophys. Res., Vol. 82, pp. 2139–2147, 1977.

4 J. M. Picone, A. E. Hedin, and D. P. Drob, "NRLMSISE-00 empirical model of the atmosphere: Statistical comparisons and scientific issues," J. Geophys. Res., Vol. 107, No. A12, 1468, doi:10.1029/2002JA009430, 2002.

5 D. Bilitza and B. W. Reinisch, "International Reference Ionosphere 2007: Improvements and new parameters," Adv. Space Res., Vol. 42, pp. 599–609, 2008.

6 B. R. Bowman, W. K. Tobiska, F. A. Marcos, and C. Valladares, "The JB2006 empirical thermospheric density model," J. Atmos. Solar-Terr. Phys., Vol. 70, pp. 774–793, 2008.

7 D. F. Heath and B. M. Schlesinger, "The Mg 280-nm doublet as a monitor of changes in solar ultraviolet irradiance," J. Geophys. Res., Vol. 91, No. D8, pp. 8672–8682, 1986.

8 J. Lean, M. VanHoosier, G. Brueckner, D. Prinz, L. Floyd, and K. Edlow, "SUSIM/UARS observations of the 120 to 300 nm flux variations during the maximum of the solar cycle: Inferences for the 11-year cycle," Geophys. Res. Lett., Vol. 19, pp. 2203–2206, 1992.

9 R. P. Cebula, M. T. DeLand, and B. M. Schlesinger, "Estimates of solar variability using the solar backscatter ultraviolet (SBUV) 2 Mg Ⅱ index from the NOAA 9 satellite," J. Geophys. Res., Vol. 97, No. D11, pp. 11,613–11,620, 1992.

10 R. Viereck, L. Puga, D. McMullin, D. Judge, M. Weber, and W. K. Tobiska, "The Mg Ⅱ index: A proxy for solar EUV," Geophys. Res. Lett., Vol. 28, pp. 1343–1346, 2001.

11 G. Thuillier and S. Bruinsma, "The Mg Ⅱ index for upper atmosphere modeling," Ann. Geophys., Vol. 19, pp. 219–228, 2001.

12 L. Floyd, J. Newmark, J. Cook, L. Herring, and D. McMullin, "Solar EUV and UV spectral irradiances and solar indices," J. Atmos. Solar-Terr. Phys., Vol. 67, pp. 3–15, 2005.

13 J. T. Emmert, J. L. Lean, and J. M. Picone, "Comment on "Oscillations of global mean TEC" by K. Hocke," J. Geophys. Res., Vol. 114, A01309, doi:10.1029/2008JA013679, 2009.

14 J. L. Lean, O. R. White, W. C. Livingston, and J. M. Picone, "Variability of a composite chromospheric irradiance index during the 11-year activity cycle and over longer time periods," J. Geophys. Res., Vol. 106, No. A6, pp. 10,645–10,658, 2001.
15 R. F. Donnelly, J. W. Harvey, D. F. Heath, and T. P. Repoff, "Temporal characteristics of the solar UV flux and He I line at 1083 nm," J. Geophys. Res., Vol. 90, No. A7, pp. 6267–6273, 1985.
16 W. K. Tobiska, S. D. Bouwer, and B. R. Bowman, "The development of new solar indices for use in thermospheric density modeling," J. Atmos. Solar-Terr. Phys., Vol. 70, pp. 803–819, 2008.
17 R. F. Donnelly, H. E. Hinteregger, and D. F. Heath, "Temporal variations of solar EUV, UV, and 10,830 - Å radiations," J. Geophys. Res., Vol. 91, No. A5, pp. 5567–5578, 1986.
18 J. Lean, "Solar ultraviolet irradiance variations: A review," J. Geophys. Res., Vol. 92, No. D1, pp. 839–868, 1987.
19 T. N. Woods, W. K. Tobiska, G. J. Rottman, and J. R. Worden, "Improved solar Lyman α irradiance modeling from 1947 through 1999 based on UARS observations," J. Geopys. Res., Vol. 105, No. A12, pp. 27,195–27,215, 2000.
20 W. K. Tobiska, T. Woods, F. Eparvier, R. Viereck, L. Floyd, D. Bouwer, G. Rottman, and O. R. White, "The SOLAR2000 empirical solar irradiance model and forecast tool," J. Atmos. Solar-Terr. Phys., Vol. 62, pp. 1233–1250, 2000.
21 S. Haykin, "Neural networks – A comprehensive foundation," Macmillan College Publishing Company, Inc., 1994.
22 G. Ma and T. Maruyama, "Derivation of TEC and estimation of instrumental biases from GEONET in Japan," Ann. Geophys., Vol. 21, pp. 2083–2093, 2003.
23 D. E. Rumelhart, G. E. Hinton, and R. J. Williams, "Learning representations by back-propagating errors," Nature, Vol. 323, No. 9, pp. 533–536, 1986.
24 L.-A. McKinnell and A. W. V. Poole, "Predicting the ionospheric *F* layer using neural networks," J. Geophys. Res., Vol. 109, A08308, doi:10.1029/2004JA010445, 2004.
25 E. O. Oyeyemi, A. W. V. Poole, and L. A. McKinnell, "On the global model for f_0F_2 using neural networks," Radio Sci., Vol. 40, RS6011, doi:10.1029/2004RS003223, 2005.
26 M. Nakamura, T. Maruyama, and Y. Shidama, "Using a neural network to make operational forecasts of ionospheric variations and storms at Kokubunji, Japan," Earth Planets Space, Vol. 59, pp. 1231–1239, 2007.
27 J.-G. Wu and H. Lundstedt, "Geomagnetic storm predictions from solar wind data with the use of dynamic neural networks," J. Geophys. Res., Vol. 102, No. A7, pp. 14,255–14,268, 1997.
28 L. G. Jacchia, J. W. Slowey, and I. G. Campbell, "An analysis of the solar-activity effects in the upper atmosphere," Planet. Space Sci., Vol. 21, pp. 1835–1842, 1973.
29 G. Paul, H. Volland, and M. Roemer, "A study of the time lag between the 27-day variations of thermospheric density and 10.7 cm solar radiation," Space Res., Vol. 14, pp. 189–193, 1974.
30 N. Jakowski, S. Heise, A. Wehrenpfennig, S. Schlüter, and R. Reimer, "GPS/GLONASS-based TEC measurements as a contributor for space weather forecast," J. Atmos. Solar-Terr. Phys., Vol. 64, pp. 729–735, 2002.
31 E. L. Afraimovich, E. I. Astafyeva, A. V. Oinats, Yu. V. Yasukevich, and I. V. Zhivetiev, "Global electron content: a new conception to track solar activity," Ann. Geophys., Vol. 26, pp. 335–344, 2008.
32 K. Min, J. Park, H. Kim, V. Kim, H. Kil, J. Lee, S. Rentz, H. Lühr, and L. Paxton, "The 27-day modulation of the low-latitude ionosphere during a solar maximum," J. Geophys. Res., Vol. 114, A04317, doi:10.1029/2008JA013881, 2009.

33 R. F. Donnelly, D. F. Heath, J. L. Lean, and G. J. Rottman, "Differences in the temporal variations of solar UV flux, 10.7-cm solar radio flux, sunspot number, and Ca-K plage data caused by solar rotation and active region evolution," J. Geophys. Res., Vol. 88, No. A12, pp. 9883–9888, 1983.
34 A. E. Hedin, "Correlations between thermospheric density and temperature, solar EUV flux, and 10.7-cm flux variations," J. Geophys. Res., Vol. 89, No. A11, pp. 9828–9834, 1984.
35 T. N. Woods, "Recent advances in observations and modeling of the solar ultraviolet and X-ray spectral irradiance," Adv. Space Res., Vol. 42, pp. 895–902, 2008.
36 J. L. Lean and A. Skumanich, "Variability of the Lyman alpha flux with solar activity," J. Geophys. Res., Vol. 88, No. A7, pp. 5751–5759, 1983.
37 J. L. Lean and T. P. Repoff, "A statistical analysis of solar flux variations over time scales of solar rotation: 1978–1982," J. Geophys. Res., Vol. 92, No. D5, pp. 5555–5563, 1987.
38 N. Jakowski, B. Fichtelmann, and A. Jungstand, "Solar activity control of ionospheric and thermospheric processes," J. Atmos. Terr. Phys., Vol. 53, pp. 1125–1130, 1991.
39 F. J. Rich, P. J. Sultan, and W. J. Burke, "The 27-day variations of plasma densities and temperatures in the topside ionosphere," J. Geopys. Res., Vol. 108, No. A7, 1297, doi:10.1029/2002JA009731, 2003.
40 P. C. Crane, L. E. Floyd, J. W. Cook, L. C. Herring, E. H. Avrett, and D. K. Prinz, "The center-to-limb behavior of solar active regions at ultraviolet wavelengths," Astronomy Astrophys., Vol. 419, pp. 735–746, doi:10.1051/0004-6361:20040012, 2004.
41 T. N. Woods, F. G. Eparvier, S. M. Bailey, P. C. Chamberlin, J. Lean, G. J. Rottman, S. C. Solomon, W. K. Tobiska, and D. L. Woodraska, "Solar EUV Experiment (SEE): Mission overview and first results," J. Geophys. Res., Vol. 110, A01312, doi:10.1029/2004JA010765, 2005.
42 T. Maruyama and M. Nakamura, "Conditions for intense ionospheric storms expanding to lower midlatitudes," J. Geophys. Res., Vol. 112, A05310, doi:10.1029/2006JA012226, 2007.
43 T. Maruyama, G. Ma, and M. Nakamura, "Signature of TEC storm on 6 November 2001 derived from dense GPS receiver network and ionosonde chain over Japan," J. Geophys. Res., Vol. 109, A10302, doi:10.1029/2004JA010451, 2004.
44 T. Maruyama, "Extreme enhancement in total electron content after sunset on 8 November 2004 and its connection with storm enhanced density," Geophys. Res. Lett., Vol. 33, L20111, doi:10.1029/2006GL027367, 2006.
45 J. Laštovička, "Forcing of the ionosphere by waves from below," J. Atmos. Solar-Terr. Phys., Vol. 68, pp. 479–497, 2006.
46 C. Borries, N. Jakowski, Ch. Jacobi, P. Hoffmann, and A. Pogoreltsev, "Spectral analysis of planetary waves seen in ionospheric total electron content (TEC): First results using GPS differential TEC and stratospheric reanalyses," J. Atmos. Solar-Terr. Phys., Vol. 69, pp. 2442–2451, 2007.

***MARUYAMA Takashi**, Ph.D. (Eng.)*
Executive Researcher
Upper Atmospheric Physics